Preprints of the 21st IFAC World Congress (Virtual)
Berlin, Germany, July 12-17, 2020

PROCESS TOMOGRAPHY FOR MODEL FREE ADAPTIVE CONTROL (MFAC) VIA FLOW REGIME IDENTIFICATION IN MULTIPHASE FLOWS

Ru Yan*, Håkon Viumdal **,
Saba Mylvaganam***

University of South-Eastern Norway, Department of EE, IT and Cybernetics, Campus Porsgrunn Norway

**ruyans@gmail.com*
*** Hakon.Viumdal@usn.no*
**** saba.mylvaganam@usn.no*

Abstract: Multiphase flows are frequently found with oil/gas/water/sand in the oil & gas industries, in processes handling dry particulates such as fluidized bed and particulate flow and slurries and sedimentation, to quote a few industrial applications. All these processes have different flow regimes with characteristic distribution of the different materials in the flow. With increasing sensor data from processes and associated possibilities for data fusion, process tomography offers non-intrusive real time sensing methods for identifying these flow regimes, which in certain cases can lead to hazards to personnel and plants in the process industries. In this paper, two scenarios of control using process tomography are presented from the oil and gas industries and powder technology. Twin plane Electrical Capacitance Tomography (ECT) with a plethora of other sensors for measuring pressure, flow rate in two phase flow involving water and air is one application. The other is particulate flow in a fluidized bed. In the case of water and air, ECT was used in a multiphase flow loop with different combinations of air and water mass flow rates enabling the generation of different flow regimes. In the case of particulate flow, different scenarios of flow conditions were generated using particulates and observing the flow regimes based on the distribution and flow rate of the particulates. For the identification of flow regimes, capacitance values from the 12-electrode ECT module at a rate of 100 frames in 200ms, were logged in for data analytics. In the final stages of using the processed data, in the case of two-phase flow 5 outputs consisting of the identified flow regimes, viz. plug, slug, annular, stratified and wavy flows were used as inputs for control and decision making. Similarly, in particulate flow ECT data were used to estimate the air velocity for fluidization as well as in identifying slug and plug flow, which are valuable to the process engineer in determining the range of air velocities for safe operation of the system used for particulate transport, often involving fluidization bed and pipelines. Tomography is used to discern features and tomometry is used in implementing the algorithms.

Keywords: Process tomography, Electrical Capacitance Tomography (ECT), sensor data fusion, flow regime, process safety, neural networks, multiphase flow, fluidized bed column (FBC), Model Free Adaptive Control (MFAC)

1. INTRODUCTION

Process tomography/tomometry can assist the measurement and control engineers in the process industries with valuable data about the process using non-invasive and non-intrusive sensors and the fusion of data from these sensors. Electrical Impedance Tomography (EIT)/ Tomometry (EITm), Electrical Capacitance Tomography (ECT)/ Tomometry (ECTm), Electrical Resistance Tomography (ERT)/ Tomometry (ERTm), have been successfully applied in the identification of different flow regimes and material distributions in multiphase flow involving liquids and gases as well as air and particulates. Abnormal and dangerous flow conditions in multiphase flow processes involving unusual distribution of materials and their velocities in the process vessels or pipelines, can in certain cases lead to hazardous conditions, which have to be detected or preferably predicted with swift and suitable response to alleviate the incumbent disasters to personnel and property. Process tomography with the combination of sensor data fusion can lead to process operations with low maintenance costs with reduced security risks to personnel. Flow conditions in processes involving multiphase flows with liquids, gas and particulates are flow regimes, volume fractions of the different phases, size of bubbles and the frequencies of their occurrences, size of slugs and the frequencies of occurrences etc. Estimation of these parameters on-line with non-intrusive sensing will help the process designers to develop sensor systems, data acquisition

from these and algorithms for alerting the process engineers, who can without delay adjust process parameters such as flow of the individual components of flow or even shut down the flow by deactivating the crucial actuators such as pumps, valves, throttles etc.

Simplified models using tell-tale values of few critical parameters, e.g. from a process tomographic module, as their inputs can help the process engineers to make decisions, to decide on a suitable and swift action. For making such decisions when the processes are running, measurement and/or soft sensor-based Model Free Adaptive Control (MFAC) algorithms are used to decide on suitable control actions, (Pradeep et al, 2012a). These methods after undergoing multiple tests can be used to design MFAC algorithms which can be supplementary to conventional control algorithms.

Processes with multiphase flow involving mixture of liquids, gases and particulates have very seldom a homogenous mixture of all these individual phases. High pressure variations involving slugs of oil/water and gas or air and particulates can lead to hazardous situations. Early warning of process parameters of flow regimes, slug size etc. in a mix indicating impending danger, can help to avoid serious damages. The process tomographic systems and techniques described in this paper show the possibilities of realizing MFAC for safer operation of processes with multiphase flows.

1.1 Multiphase rig for two phase (air/water) flow

A simplified P&ID diagram of a multiphase flow loop for generating desired flow regimes with air, water and oil as the phases in the flow is shown in Fig. 1, which shows the sensors and actuators relevant monitoring and generating the relevant flow regimes.

Two Coriolis flow meters ('FT') with an uncertainty of ±0.01kg/min, are located immediately before the ECT module, for measuring mass flow rates of air and water. Differential pressure transmitters ('PDT') are used for monitoring the pressure drop between the ends of the test section with the ECT module. The gamma radiation meter ('GD') estimates the phase fraction over the pipe cross-section based on the differing absorption coefficients of air, water and oil. The control valves and pumps constitute the actuators in the system and adjusts the amount of each phase to attain various compositions of the phases, i.e. fractions of oil, water and air. From extensive tests run with different fractions of oil, water and air, different desired flow regimes can be generated in the rig. For the two-phase flow studies with air and water, the test matrix with the details of air and water flow rates leading to various flow regimes are presented in (Johansen et al, 2018).

1.2 Particulate flow

A fluidized bed column (FBC) used in this study for observing fluidization of particles and their flow in a vertical pipe section with focus on the flow regimes is shown in Fig. 2. The focus in the usage of ECT module in these tests are to identify the regimes fixed bed, fluidisation and slugging. For these three flow regimes, starting point of fluidization and air inflow velocity for generating bubbling flow can be observed through the vertical transparent pipe section.

Based on these observations, control methods based on air inflow velocity can be developed for generating different flow regimes. The vertical FBC used in this study with the twin plane ECT-module is shown in Fig. 2. with a corresponding schematic diagram showing the major modules in Fig. 2. (right).

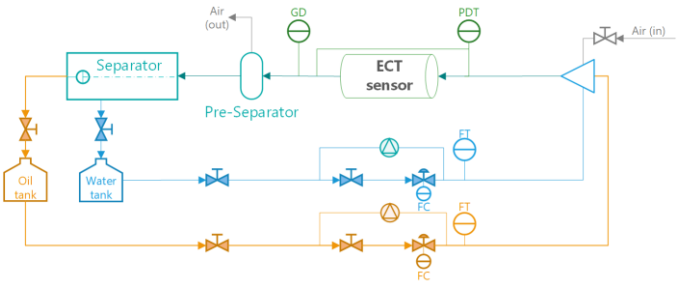

Fig. 1. P&ID for the flow rig with ECT-module, sensors and actuators. This paper focusses on two phase flow with air and water. Tests performed at room temperature and atmospheric pressure. FT/FC-Flow Transmitter/Controller, GD – Gamma Radiation Meter for density measurements, PDT-Differential Pressure Transmitter

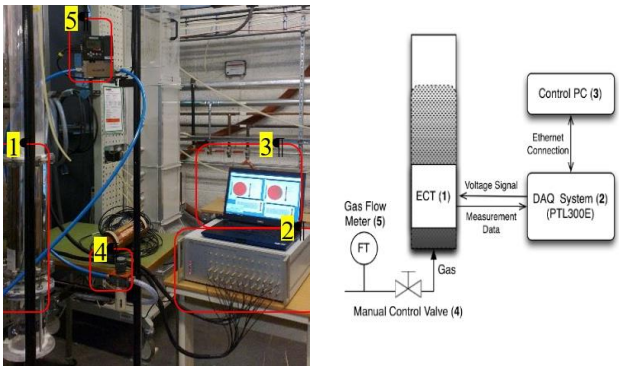

Fig. 2. Picture of FBC and ECT -module. Schematic diagram of the FBC with installed twin plane ECT sensor (right).

2. ECT MEASUREMENTS

In both systems shown in Fig. 1 and Fig. 2, the ECT-modules give an array of capacitance values. An ECT module usually has all the electrodes distributed along the periphery of the pipeline. For an ECT-module with N-electrodes in one plane, a typical set of normalized capacitance measurements can be presented in a matrix form as:

$$CN(i,j,t) = \begin{cases} CN(i,j,t), & i < j \\ 0, & i \geq j \end{cases} \quad (1)$$

where CN is the normalized capacitance measurements; $i = 1 \ldots, N; j = 1, 2, \ldots, N$ and t represents time.

Equation (1) leads to a $N \times N$ upper triangular matrix with zeros on its diagonal elements, since typical ECT measurement

systems skip the repetitions of the same inter-electrode combinations, because at any instant t, $C_{ij}(t) = C_{ji}(t)$, for the raw capacitances measured at any two electrodes i and j of the ECT-module. Thus, for a set of measurements, usually called a "frame", the complete capacitance matrix is given by:

$$CN(t)_{(u,v)} = \begin{cases} CN(i,j,t), & u \le v; \quad i = u; \quad j = N + u - v \\ CN(j,i,t), & u > v; \quad i = N - u + v; \quad j = v \end{cases} \tag{2}$$

where, u and v are the index of row and column in the matrix respectively, $u = 1, \ldots, (N\text{-}1)$; $v = 1, \ldots, (N\text{-}1)$.

Different approaches are presented in this paper for fusing these raw capacitance data for a MFAC of multiphase flow of liquids, particulates and gases/air. One method is based on using these data from each frame as inputs to a neural network and fusing the data to get the flow regimes as the output. The other method is based on calculating the eigenvalues of $(N\text{-}1) \times (N\text{-}1)$ and taking the leading eigenvalues from the matrices for all the frames analyzed. The maximal eigenvalues in each vector is pointed out as the leading eigenvalue of each corresponding capacitance measurement frame. The work by Fang & Cumberbatch (2005), opened a new direction in EIT generally and reinforced the concept of ECTm.

The third method is based on using k- Nearest Neighbour (k-NN) algorithms. The fourth method is using cascades of Support Vector Machines (SVM)

3. FLOW REGIME IDENTIFICATION

3.1 Water-air flow in a horizontal pipe

In monitoring and control of multiphase flow in the oil and gas industries, accurate information of the the flow regimes helps the process engineers to be prepared to handle unusual pressure build-up due to the occurrence of large bubbles, the sizes of which could extend to hundreds of pipe diameters, (Wang et al, 2006). These unusually large bubbles, plugs, and slugs in multiphase flow can lead to the creation of high-pressure zones in the pipeline. Because of such high-pressure zones, the pipelines and their supporting structures can break down. Fig. 3 shows the frequently encountered multiphase flow regimes including bubbles, plugs, slugs, wavy and annular flows in horizontal pipelines, (Thome, 2004).

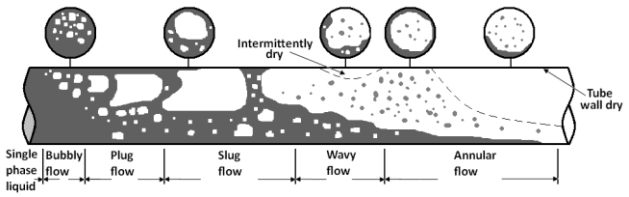

Fig. 3. Commonly encountered flow regimes in horizontal multiphase flow, Thome (2004) and modified.

3.2 Fluidised Bed Columns and Particulate Transport

Similarly, in particulate transport involving fluidized bed, as shown in Fig. 4, the transition zones travers the pattern of starting with packed bed, via bubbling/slugging, turbulent and fast fluidization regime and finally leading to the pneumatic transport of the particulates.

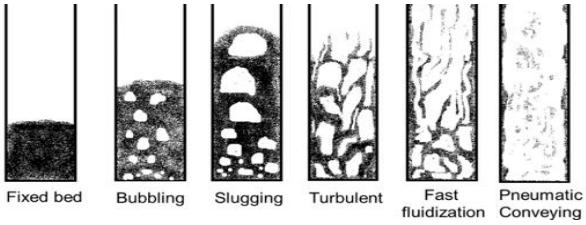

Fig. 4. Commonly encountered *flow* regimes in particulate flow in fluidized bed columns (FBC), Yan (2016).

4. DETECTION OF FLOW REGIMES

In this section, some techniques will be presented for analysing the ECT data to identify flow regimes and if necessary, image the flow phenomena. Both multiphase flow with air and water and particulate flow involving FBCs are taken as case studies for non-invasive flow regime identification and as an immediate follow-up initiating MFAC of the processes for avoiding hazardous situations. Autonomous and timely detection of flow regimes and the transition zones between some of them non-invasively using ECT can help to design MFAC algorithms which can be used along with other algorithms. In earlier works, applying regression and prediction techniques with artificial neural networks, good results were achieved for selected parameters such as level of liquid, gas etc. in static multiphase studies using stationary pipe sections with ECT. Using pilot scale multiphase flow experiments with a dedicated multiphase rig and FBC for particulate flow studies, this work has focused on flows involving at times some complex transitions between flow regimes, using advanced neural network structures for pattern recognition and clustering.

4.1 Identification of Flow Regimes in Air-Water Two Phase Flows in Horizontal Pipelines

Artificial neural networks are used for developing soft/virtual sensors and exhibit enhanced ability to mask spurious effects due to unwanted /unimportant parameters. In recent years, due to improvement of hardware with respect to processing speed and memory capacities, and enhanced neural network training algorithms, deep learning (DL) is becoming more and more popular. DL has become one of the main drivers in many new applications in almost all fields.

Deep Belief Network (DBN) belongs to the category of deep learning models and is used to extract representative features in a data set. By using DBN, a model free multiphase flow regime identifier can be developed as schematically illustrated in Fig. 5.

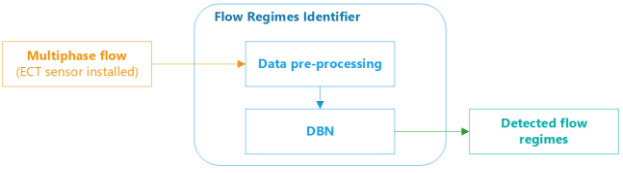

Fig. 5. DBN based flow regime identifier in MFAC mode using ECTm.

4.1.1 Construction of DBN

DBN is a composition of series fully connected Restricted Boltzmann Machines (RBM). RBM is a shallow neural network that only consists two layers: visible/ input layer and hidden layer. The energy function E given in (1) describes the system stability, with lower energy associated with optimized parameters, weights and bias etc. of RBM, (Hinton, 2010).

$$E(v,h) = -\sum_{i\,\epsilon\,visible} a_i v_i - \sum_{j\epsilon\,hidden} b_i h_i - \sum_{i,j} v_i h_j w_{ij} \quad (3)$$

where v_i, h_j are the states variables of visible unit i and hidden unit j respectively; a_i, b_j are the corresponding biases with w_{ij} the weights between the visible and hidden unit. The objective of the training of RBM is to achieve the optimised parameter set $\{a_i,\ b_j,\ w_{ij}\}$.

In a DBN, RBMs are connected in series, as shown in Fig. 6(b) with 2-hidden layers of DBN, where the outputs from the hidden layers in the previous RBM will be the inputs to the visible layer of the following RBM. By combing these RBMs, the DBN functions as an effective multilayer feature extractor capable of recognizing inherent patterns in big data.

4.1.2 Pre-processing the Measurement Data

Since each flow regime is a continuous phenomenon in space and time, to identify these flow regimes correctly, each sample of the time series fed into the neural network should contain enough information with good both spatial and temporal resolutions. The technical specification of ECT system discussed in this paper is given in Table 1.

Table 1: ECT Module technical specifications

ECT sensor	• Single plane; • 12 electrodes per sensor plane; • (66 individual capacitance measurements in each frame).
Sampling frequency	• 500 frame per second

Per training sample with 00 frames (obtained in 0.2s), there are 6600 capacitance values, implying 6600 neurons at the input layer of the DBN. This large number will, in a time consuming and low efficiency training, put heavy demands on the system memory. Therefore, prior to the training of DBN, dimensional reduction of the inputs from each frame is necessary.

The method used here for the reduction of dimensions employs statistical analysis of the ECTm data as they are gathered. The mean value (Pm), quantiles (Pqua) at [0.1, 0.25, 0.5, 0.75, 0.9] and kurtosis (Pkur), leading to a total of 7 variables are used to represent the 66 measurements per frame, thus reducing the data almost by a factor of 10. Each training sample has 100 frames, thus the total number in each training sample is reduced from 6600 to 700, as illustrated in Fig. 6(a).

The DBN used consists of 2 RBMs. The structure of the DBN is given in Fig. 6(b). In the 1st RBM, there are 200 neurons in the hidden layer. In the 2nd RBM, the number of neurons in its hidden layer is set to 100. Finally, the hidden layer output form 2nd RBM is fully connected to a feedforward neural network with 5 neurons (to represent five different flow regimes) in the output layer.

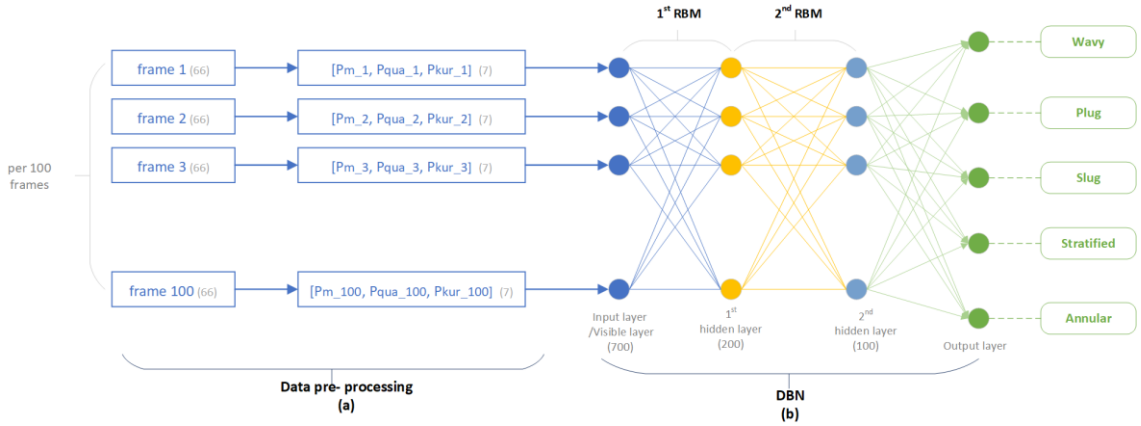

Fig. 6. (a) Pre-processing of ECT data for deep learning analytics for real time flow regime identification; (b) Structure of DBN with two RBMs. 700 neurons as inputs with the capacitance values from 100 frames and 5 different flow regimes as outputs.

4.1.3 Training of DBN and results

The process of DBN training can be divided into two phases: pre-training (unsupervised) and fine-tuning (supervised), with the following steps:

- Training: 1st RBM until it reaches stability; then fix the achieved weights and biases for this RBM.
- Training 2nd or the following RBM: use the outputs from previous RBM's hidden layer, as inputs. Then training the RBM until it reaches stability. After training, the optimised weights and biases are selected.

- Fine-tuning: Adding an output layer, see the output layer Fig. 6(b); perform supervised training of the whole DBN by using forward propagation - backpropagation method to update the weights and biases as training normal feedforward neural network.

During the RBM training process, from step 1) and 2), the updating algorithms for the parameter set $\{a_i,\ b_j,\ w_{ij}\}$ are given in (4) - (6).

$$\Delta a_i = \eta(\langle v_i \rangle_{data} - \langle v_i \rangle_{model}) \quad (4)$$

$$\Delta b_j = \eta(\langle h_j \rangle_{data} - \langle h_j \rangle_{model}) \quad (5)$$

$$\Delta w_{ij} = \eta(\langle v_i h_j \rangle_{data} - \langle v_i h_j \rangle_{model}) \quad (6)$$

where Δ indicates the changes in $a_i,\ b_j,\ w_{ij}$ after each training epoch; η is learning rate; $\langle . \rangle$ indicate reconstructed sample at corresponding hidden layer, h, and visiable layer, v. In step 3), the activation function used for output layer is logistic sigmoid function, given in (7).

$$f(x) = \frac{1}{1+e^{-x}} \quad (7)$$

The total data set is divided into two main parts: training & validation set and test set. For the training & validation dataset, the necessary measurements are taken for similar inlet flow conditions. 80% of the training & validation data were used for training, and the remaining were used for validation. Further, to verify its robustness, the trained model was tested by using the test data set from different in-let flow conditions.

4.2 Identification of Flow Regimes in Fluidized Beds

Fig. 7 shows the reconstructed 3D images of the bubble movement under different air inflow conditions. From the reconstructed movements of bubbles presented in Fig. 7, in the first three experiments (at airflows from 290 to 329 SLM) can be identified as 'bubbling' regime. However, already during the 3rd experiment, features indicating 'slugging' can be observed. From the 4th experiment (at an airflow of 340SLM), the flow has a transitional tendency from 'bubbling' to 'slugging'. When the airflow increased to 380SLM and to even higher speeds (from 8th to 12th experiment), the bubbles tend to occupy almost the entire cross section of the sensor plane. The flows corresponding to those observed during the 8th to 12th experiments belong to the 'turbulent' and 'fast fluidization' regimes.

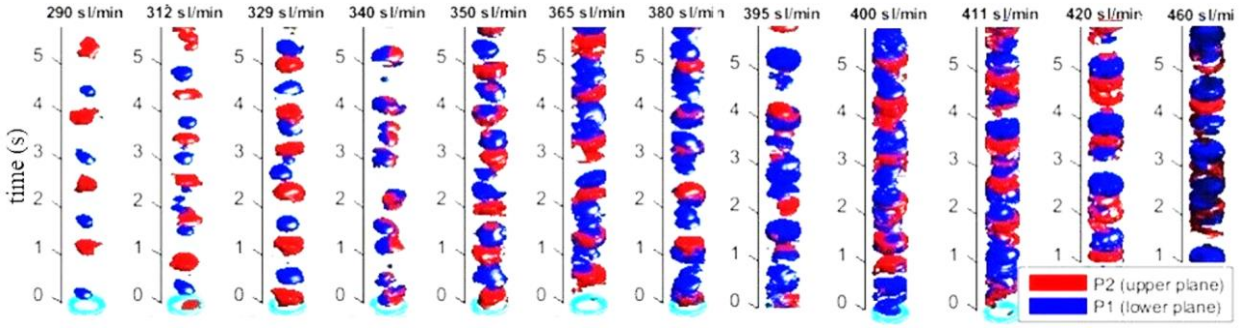

Fig. 7. Reconstructed bubble images with airflow varying from 290 to 340 SLM. 'blue' indicates the bubble generated from the lower ECT sensor plane (p1, relatively close to the bottom of FBC and air inlet area); 'red' indicates the bubble generated from upper ECT sensor plane (p2). Adapted from Yan et al (2019).

4.2.1 Identification using Leading Eigenvalues

Fig. 8 (a) shows the variations of the RMS values of the ratio of the leading eigenvalues at planes p1 and p2. As can be seen, in the first 3 experiments, the RMS values do not increase much; from the 4th to 7th experiments, the RMS values increase significantly with increasing air inflow velocity; from 8th to 10th experiments the RMS values are more stable again until to the last two experiments.

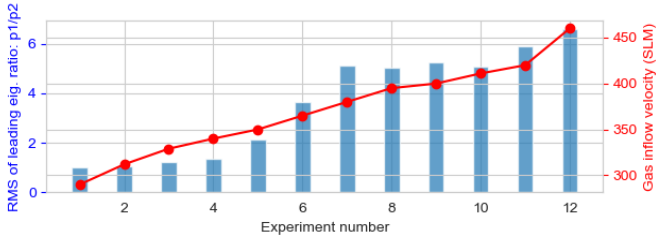

(a)

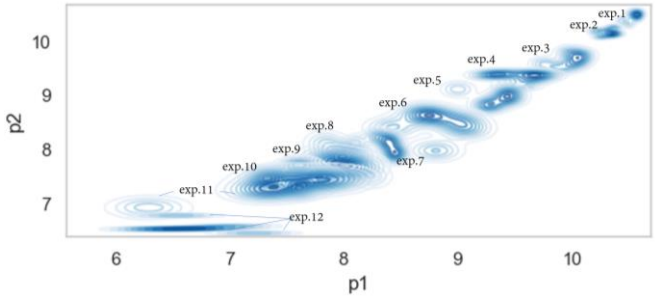

(b)

Fig. 8. (a) RMS of the ratios of leading eigenvalues for capacitance matrices measured at p1 and p2; the red dot-line plot is the corresponding air velocity; (b) KDE plot: Data distribution of 10-sec averaged leading eigenvalues between p1 and p2.

Fig. 8 (b) shows the Gaussian Kernel Density Estimate (KDE) plot, which shows the distribution of 10 second averaged

leading eigenvalues between the two sensor planes P1 and P2. The KDE curves from each experiment show clusters with the following pattern:

- Group 1: first two experiments are in this group;
- Group 1-2 (transition): from the 3rd experiment, the KDE curve starts to 'connect' to the next one;
- Group 2: from the 4th experiment, the KDE curves shows more clustering with "centers";
- Group 3: from the 7th experiment, the KDE curves start to overlap each other;
- Group 4: from 11th to 12th experiment, isolated islands (cap) is formed with respect to the other KDE curves.

From these clusters by using KDE and leading eigenvalues, the raw capacitance values help to form the capacitance matrices for each frame, whose leading eigenvalues show characteristic patterns showing significant "fingerprint" behaviour, which can be associated with the different flow regimes. Fusion of these data features can enhance the identification process.

However, for a reliable control of the particulate flow behaviour in the FBC, the above observations are not enough for using them as inputs to the control system. Therefore, in the following sub-section 4.2.2, the classification results by using SVM are given.

4.2.2. k-NN vs Stacked SVM model

Since there are mainly three types of flow regimes of interest in the context of this study, viz. 'bubbling', 'slugging' and 'turbulent to pneumatic' conveying, we need soft-sensing strategies to identify non-intrusively using the ECT system.

Using k-Nearest Neighbor (k-NN) method for classification with Minkowski distance, number of neighbors: 2, 3, 6, 7 and weights of each points: uniform weights; weighted equally, we get the nice classification shown Fig. 9. The inputs to k-NN are: X: one second averaged leading eigenvalues pair: ['p1', 'p2'] and Y (target): 1 / 'bubbling'; 2/ 'slugging' and 3 /'others').

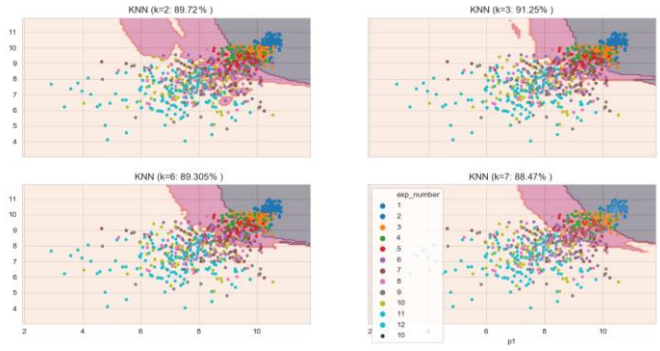

Fig. 9. Classification using k-NN showing the different regimes according to the numbering scheme used for the experiments with characteristic flow regimes.

Achieved accuracies are given in Table 2. The highest accuracy is for 'k=3'. However, as can be observed in Fig.9, the model overfits the data. The model with 'k=6' gives higher accuracy without overfitting.

Table 2: Accuracy of k-NN model at different k numbers

	k=2	k=3	k=6	k=7
Accuracy	0.90	0.91	0.89	0.88

Similarly, in the results shown in this section, a stack-SVM (composed of two individual SVMs), radial basis function (RBF) kernel, is trained. In this stack of two blocks of SVM, two separate SVMs are used to classify 'bubbling / not bubbling' and 'slugging / turbulent and else' successively as illustrated in Fig. 10.

For providing a 'quick response', the leading eigenvalues are averaged per second instead of 10 seconds (used in the case of KDE of Fig. 8(b)). The inputs to stack-SVM are leading eigenvalues from lower sensor plane (p1) and upper sensor plane (p2), averaged over a period of one second. In Fig. 10, the dot size is dependent on the difference between the corresponding leading eigenvalues at the planes, p1 and p2.

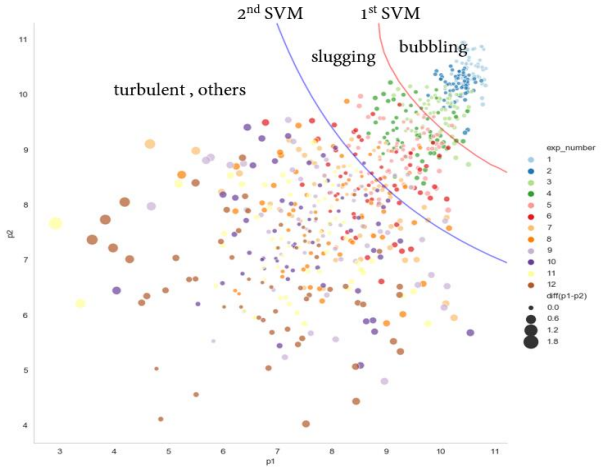

Fig. 10. Overview of trained stacked SVM results; where 1st SVM (red hyperplane) is used to classify 'bubbling' and others; 2nd SVM (blue hyperplane) is used to classify between 'slugging' and 'turbulent, others'.

The hyperplanes from the stack-SVM are also presented in Fig. 10. The first SVM gives an accuracy of 95.6%; and the second SVM gives an accuracy of 91.2%; the total stack-SVM gives an accuracy of 87%.

The first SVM (red hyperplane) is for recognition if the regime is 'bubbling' or not, performing at an accuracy of 95.6%; the second SVM (blue hyperplane) is for identifying the flow regime of 'bubbling & slugging' or 'turbulent, others', giving an accuracy of 91.2%.

The combination of the first SVM and the second SVM, gives for all these three flow regimes of interest an accuracy of identification of 87 %. This is an acceptable result, especially as there are unclear transitions between the three flow regimes under scrutiny.

In summary, the k-NN model can provide a bit higher accuracy (approx. 2% in this case) than the SVM model. While, due to the differences in the working mechanisms of k-NN and SVM, training and running of SVM model is simpler than k-NN model. SVM uses smaller training set (support vectors) and

needs less computation power. Training the k-NN model using different *k* numbers for determining the "best value" for *k* is a computationally demanding process, especially for a large dataset. In field applications, the SVM model has quicker response than that of k-NN model. Therefore, for the current application, the SVM model is a more suitable solution than the k-NN model.

5. MFAC USING TOMOGRAPHY

5.1 Flow regime identification and control of multiphase flow

By using a DBN to process the measurements from a single plane ECT sensor, the frequently encountered flow regimes, plug/ slug/ annular/ stratify/ wavy, can be identified with high accuracy, see Table 3. Based on all training / validation / test results, categorizing both 'Slug' and 'Plug' as a single regime (e.g. 'large bubble'), the identification accuracy is above 86%, (86% from training results, 100% from validation results and 96% from test results). These techniques do have some wrong identifications, which are almost intrinsic due to the similar features of some of the flow regimes.

Table 2: Accuracy of DNN model from training, validation and testing

	Plug	Slug	Annular	Stratified	Wavy
Training	0.77	0.84	1	0.98	1
Validation	0.71	0.85	1	1	0.95
Test	0.88	0.84	1	0*	1

*all being misclassified to 'wavy (92%) and 'slug' (8%)

From the validation and test results, 14% and 4% of samples of 'Slug' flow have been misclassified as either 'Stratified' or 'Wavy' flows, due to the similarity of their features found in short time-windows of 0.2 second. Due to the same reason, from the samples of 'Stratified' flow, 92% of them has been misclassified as 'Wavy' and 8% been misclassified as 'Slug'. This type of misclassification can be easily avoided, by fusing the data from the differential pressure measurements, 'DP' in Fig. 1, since there are significant differences between DP measurements during intermittent and relatively stable flow conditions.

By using ECTm data as inputs to DBN and pressure measurements, a model free adaptive controller (MFAC) can be easily implemented in processes involving multiphase flows. In a conventional model based predictive control (MPC) the functioning of the MPC heavily relies on the accuracy of the model and control algorithms. In fact, in many applications, due to the substantial number of parameters involved in multiphase flow-based process, designing an MPC to tackle all flow conditions is a big challenge. In comparison, Fig. 11 presents the configuration of a MFAC based on DBN, which doesn't require any dedicated model. By changing the strategy from MPC to MFAC control or to a workable blend of MPC and MFAC, the process engineer will have an increased advantage in preventing hazards.

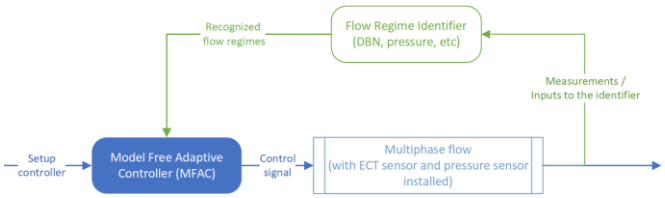

Fig. 11. Flow chart of FBC controller design scenario based on a signal plane ECT sensor based on some machine-learning algorithms.

5.2 Flow regime identification and control of FBC

Using variations in ECT image pixel data, a stack of 3D images of bubbles is reconstructed using, time series from both sensor planes in a twin plane ECT-module. From these reconstructed 3D images, the difference between various flow regimes can be observed and identified with good accuracy. This is a method based on image processing.

The bubble velocity and bubble frequency are estimated using the CVR data from both ECT sensor planes. From the results based on this method, we find that this method can be applied to identify bubble characteristics and bubble coalescence numerically. Further, using a stack-SVM, the main fluidizing flow regimes can be identified through clustering the pattern from the averaged volume ratio from both sensor planes. The stack-SVM classification / identification results can deliver a unique output, such as a single number (index), e.g. '1' for bubbling, '2' for slugging, and so on. Therefore, the stacked SVM method has the potential for applications in real time control of processes involving FBC.

These results give useful information in identifying bubble velocity, frequency, location, coalescence and fluidization and flow regime identification. Thus, we suggest an automatic in-line real time control strategy of processes involving FBC based on these machine-learning methods as illustrated in Fig. 12.

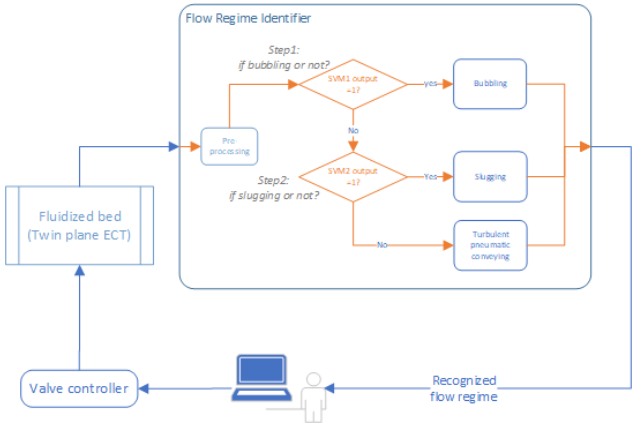

Fig. 12. Flow chart of an FBC controller design scenario based on ECT sensor based on some machine-learning algorithms.

Fig. 13 shows a scenario of using the ECT data by fusing them with conventional sensor data usually available in the process industries. The system architecture suggested in Fig. 13 has

been realized in conjunction with the two processes described in this paper. A cross-platform application involving LabVIEW and DELTA V has been also realized for robotic applications. Just for illustrations, MATRIKON OPC server is selected for this application.

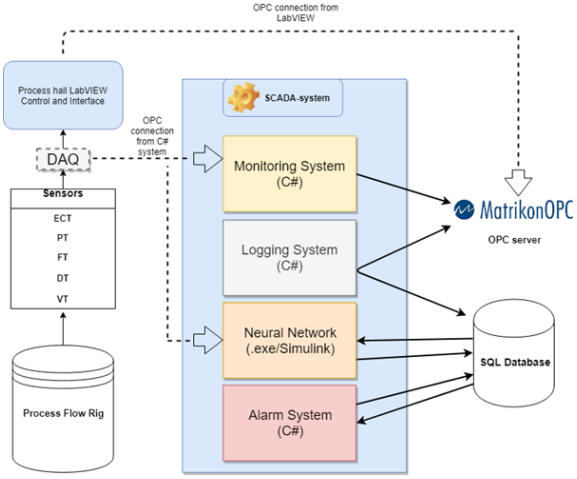

Fig. 13. Flow chart of a MFAC with the main components - design scenario based on ECT sensor and other sensors, Courtesy, Aleksander Tokle Poverud, USN. A scenario relevant to the process industries. ECT-Electrical Capacitance Tomograph, PT-Pressure Transmitter, FT- Flow Transmitter etc. Python is increasingly used in the process industries for some of the tasks listed here.

6. CONCLUSIONS

The pilot scale multiphase flow rig and the fluidised bed column have been used as typical examples of using data from ECT modules for identifying flow regimes and using these data in detecting operational hazards. With the ever-increasing use of cloud services for computing and developments in near sensor signal processing techniques, these methodologies open a machine learning approach to MFAC using raw data from the sensors used in the process and data from process tomographic modules. As shown in Fig. 12, these routines can be integrated in the already existing systems used for process measurements and control.

The approach presented here using MFAC falls under the class of "black-box models", used in complex non-linear process modeling and can be enhanced by explainable machine learning approaches involving "gray box models", with inputs from well proved models, at least partly describing the process. In an earlier work, ECT data have been used to enhance the CFD modeling of three phase flow, Pradeep et al, 2012b. The approach presented here is easy to use, and the necessary codes can be adapted quickly with the swift updating of the codes to address newly found features.

This paper presents the possibility of using process tomography for MFAC, based on some publications of its authors in the tomographic literature. There are already elements of the strategies discussed here used in predictive maintenance.

ACKNOWLEDGMENT

Multiphase experiments with an array of multi-modal sensors including the EIT, ECT and GRM was done in the process lab at University of South-eastern Norway (USN) with the help of Senior Engineer Fredrik Hansen and master student Aleksander Tokle Poevrud. The experimental campaign was partly financed by the Self Adapting Model-based system for Process Autonomy (SAM) project supported by Research Council of Norway and the process industries (Project No. 295945)

REFERENCES

Fang W. and Cumberbatch E. (2005) Matrix properties of data from electrical capacitance tomography, Journal of Engineering Mathematics vol.51, p. 127-146

Hinton G. (2010) "A Practical Guide to Training Restricted Boltzmann Machines", Version 1, Department of Computer Science, University of Toronto

Johansen, R., & Østby, T. & Dupre, A. & Mylvaganam,(2018). "Long Short-Term Memory Neural Networks for Flow Regime Identification Using ECT", 9th World Congress in Industrial Process Tomography Bath UK.

Pradeep, C. & Ru, Y., Mylvaganam, S., (2012a), "Neural Network-Based Interface Level Measurement in Pipes Using Peripherally Distributed Set of Electrodes Sensed Symmetrically and Asymmetrically", Instrumentation and Measurement, IEEE Transactions, Vol. 61. 2362-2373. 10.1109/TIM.2012.2199191.

Pradeep, C. Yan, R. & Vestol, S. & Melaaen, M.C., Mylvaganam, S., (2012b), "Electrical Capacitance Tomography (ECT) and gamma radiation meter for comparison with and validation and tuning of CFD modeling of multiphase flow", Measurement Science and Technology. 25. 45-50.

Thome J. R. (2004) "Engineering data book III," Wolverine Tube Inc.

Wang X., Guo L. and Zhang X. (2006) "Development of Liquid Slug Length in Gas-Liquid Slug Flow Along Horizontal Pipeline: Experiment and Simulation". Chinese J. Chem. Eng., vol.14 (5), p 626- 633.

Yan R. (2016), "Usage of Process Tomographic Techniques in Study of Flow Dynamics in Fluid and Particulate Flow", PhD Thesis, University of South-Eastern Norway.

Yan, R., Sharma, R., Viumdal, H., Mylvaganam, S., (2019), "SOFT SENSING with ECT in Particulate Transport with Focus on Bubble", 19th International Conference on Transport & Sedimentation of Solid Particles, Cape Town, South Africa.